ROYAL SOCIETY OPEN SCIENCE

royalsocietypublishing.org/journal/rsos

CC BY

Research

Cite this article: King BF, Peck LS, Harper EM. 2026 Mineralogy and organic content are major predictors of shell loss in bivalves under reduced salinity, ocean freshening conditions. *R. Soc. Open Sci.* **13**: 251473.
https://doi.org/10.1098/rsos.251473

Received: 5 August 2025
Accepted: 25 November 2025

Subject Category:
Organismal and evolutionary biology

Subject Areas:
environmental science

Keywords:
biomineralization, dissolution, salinity, mollusc, climate change, solubility

Author for correspondence:
Bethany F. King
e-mail: bfk24@cam.ac.uk

Supplementary material is available online at.
https://doi.org/10.6084/m9.figshare.6025748

THE ROYAL SOCIETY PUBLISHING

Mineralogy and organic content are major predictors of shell loss in bivalves under reduced salinity, ocean freshening conditions

Bethany F. King[1,2], Lloyd S. Peck[2] and Elizabeth M. Harper[1,2]

[1]Department of Earth Sciences, University of Cambridge, Cambridge, UK
[2]British Antarctic Survey, Cambridge, UK

BFK, 0009-0007-3462-0127; LSP, 0000-0003-3479-6791; EMH, 0000-0002-1092-3867

Ocean freshening due to increased precipitation and ice melting in a warming world poses a significant threat to marine calcifiers. The reduced availability of calcification substrates and an undersaturated calcium carbonate state challenge shell construction and maintenance. The corrosive potential of ocean acidification on biomineralized skeletons is well understood, but few studies have investigated the corrosive potential of significant freshwater input into marine habitats. To examine the susceptibility of invertebrate biocomposites to low salinity, we exposed blocks containing polished surfaces of pristine shell material of six bivalve taxa, representing different mineralogies and microstructures, to a salinity gradient (0–45‰) for 180 days. By measuring the loss of shell thickness, we revealed a significant correlation between dissolution and decreasing salinity. Significantly different amounts of shell thickness loss were observed across microstructures, revealing mineralogy and organic content as important predictors for dissolution. Aragonite layers lost significantly more shell thickness than calcite, and higher organic content retarded dissolution across microstructures. Overall, shell dissolution at low salinities is significant and comparable to dissolution predicted under end-of-century ocean acidification scenarios. The compromised integrity of marine invertebrate biomineralized skeletons because of ocean freshening is of critical concern with future predicted increases in precipitation and sea ice melt.

© 2026 The Authors. Published by the Royal Society under the terms of the Creative Commons Attribution License http://creativecommons.org/licenses/by/4.0/, which permits unrestricted use, provided the original author and source are credited.

Downloaded from http://royalsocietypublishing.org/rsos/article-pdf/doi/10.1098/rsos.251473/5634029/rsos.251473.pdf
by guest
on 23 January 2026

1. Introduction

Salinity is a key factor in determining ecosystem structure and function, limiting organisms at their physiological and ecological thresholds [1–3]. Salinity gradients are particularly prominent in coastal environments influenced by seasonal and tidal cycles, in addition to significant terrestrial freshwater runoff at the river–sea interface [4]. Global annual maximum daily precipitation levels have increased by an average of 5.73 mm (8.5%) over the last century [5] and precipitation extremes are predicted to increase by approximately 6–30% under low- and high-emission scenarios, respectively, by 2100 [6]. These enhanced levels of rainfall simultaneously increase flooding and freshwater runoff [7,8]. Chronic freshwater input significantly impacts marine ecosystems, with recognized consequences on the growth and reproduction of organisms, as well as increasing mortality events [7,9,10]. The implications of freshwater input are exacerbated where land and sea meet, compromising coastal lagoon, estuarine and nearshore ecosystems [11,12]. The isolated nature of coastal lagoons and limited input of seawater increase their vulnerability of evolving into a freshwater habitat [13]. Home to a specialist fauna that provide ecosystem services and serve as key food sources for migrating birds and invertebrates, the consequences of freshening impacts could be extensive [14].

Unsustainable, human-driven energy and land use continue to drive global greenhouse gas emissions to record-breaking levels yearly [15]. This has contributed to a 0.8–1.3°C increase in global surface temperatures above preindustrial levels [16]. With every 1°C of warming, atmospheric moisture increases by approximately 7%, driving more intense and severe precipitation events [17–19]. As much as 80% of freshwater exchange (precipitation and evaporation) occurs over the ocean, and shifts in this hydrological cycle are reflected by changes in salinity [20,21]. Increased summer melt of the cryosphere exacerbates freshening at higher latitudes, while at warmer, lower latitudes, where evaporation exceeds rainfall, conditions are becoming more saline [22–26]. Regional differences in salinity are predicted to become further amplified [16,20].

Molluscs are a large and diverse phylum that make up 23% of the extant marine fauna [27]. Although some molluscs have lost their shells, and others have internalized them, most molluscs biomineralize external calcium carbonate skeletons. As with all calcifiers, shifts in salinity will impact the shelled molluscs as the manufacture and maintenance of their biomineralized shells become increasingly more difficult with decreasing salinity [3]. The availability of calcium [Ca^{2+}] and bicarbonate [HCO_3^-] ions, the essential building blocks needed for $CaCO_3$ biomineralization, declines linearly along a decreasing salinity gradient [3]. Limited further by reduced epithelial ion transport and kinetic constraints, the energetic costs of biomineralization increase significantly [3,28,29]. Reduced salinity also critically affects the ability to maintain a shell once formed as the undersaturated $CaCO_3$ state ($\Omega \leq 1$) also promotes the dissolution of pre-existing calcium carbonate biominerals [3,30]. Some species of shell-bearing molluscs have adapted to corrosive undersaturated conditions by having a thickened, persistent periostracum, the external waterproof organic layer on the surface of the shell, whose principal function is as a template for shell formation but which also serves as a frontline defence against dissolution [31,32]. Nevertheless, the protective properties of the periostracum, however thin, may become compromised through decay, damage or wear [33].

Salinity is a key predictor of shell shape, composition and formation in mussels and oysters [34–36], and molluscs have been shown to initiate compensatory biomineralization processes in response to biotic and abiotic stressors [3,35,37–40]. A number of traits have been postulated as adaptations against shell dissolution, for example, a thicker periostracum and intra-shell organic layers in brackish and freshwater taxa [41,42], increased thickness of periostracum and proportions of calcite and organic matrix in *Mytilus* species [38,41], and it has been suggested that the periostracum of the estuarine neritid gastropod *Neripteron violaceum* is chemically adapted to encourage the adhesion of clay minerals to act as an additional barrier to dissolution [43]. Most research on the dissolution of $CaCO_3$ skeletons in a range of invertebrate taxa has primarily focused on the adaptations of freshwater molluscs [41,44–46] and acidifying oceans [47–52]. However, studies investigating the effects of varying salinity on biomineralization in brackish and low-salinity environments are now emerging [35,38,53].

Bivalves are the second largest class within the phylum Mollusca and are a key foundation group in coastal marine ecosystems, providing community and regulatory services [54,55]. With an estimated market value of $17.1 billion globally, they are also of high economic importance [56]. Bivalves in these dynamic environments generally demonstrate euryhalinity and have evolved behavioural and physiological responses to withstand salinity fluctuations [57,58]. The calcium carbonate shells of bivalves are highly diverse and serve a multitude of functions, well adapted to the external

Downloaded from http://royalsocietypublishing.org/rsos/article-pdf/doi/10.1098/rsos.251473/5634029/rsos.251473.pdf
by guest
on 23 January 2026

requirements of the habitat and life mode [59]. Providing skeletal support for the soft tissues inside, as well as protection from predation and unfavourable external conditions, the shell is vital to their survival. Shell integrity is likely to be compromised with episodes of coastal freshening, as the ratio of optimal calcification substrates deviates in hyposaline conditions [3,28].

Within Bivalvia, a number of shell microstructures are defined by the arrangement of the mineralized and organic biocomposites [60,61]. Different microstructural arrangements demonstrate a range of mechanical qualities, with variations in hardness, elasticity, strength, density and resistance to dissolution strongly correlated with life mode [47,62,63]. The biocomposite shells generally consist of 95.0–99.9% calcium carbonate and 0.01–5.0% organic matrix, though organic proportions as high as 16.11% have been reported in very specialized microstructures [64,65]. Aragonite is the dominant polymorph of calcium carbonate used and, although no taxa are exclusively calcitic, several bivalve taxa secrete an outer calcite layer [62]. Inorganic aragonite is more soluble than calcite, but both are increasingly susceptible to dissolution at lower salinities, temperatures [66] and pH [47]. The resilience of each polymorph to dissolution is also influenced by additional factors, such as crystal size, the proportion of organic matrix and Mg : Ca ratio [47,62]. As well as providing structural reinforcement and serving as a template for biomineralization, the organic matrix may play a role in shell deterioration, either by initially shrouding the individual crystals it envelopes from unfavourable conditions, encouraging dissolution directly in altered conditions [67] or by serving as a microbial substratum [68]. Meanwhile, the substitution of magnesium in place of calcium in calcite (the aragonite structure does not easily tolerate the incorporation of small Mg^{2+} ions) alters the thermodynamic properties of calcite, increasing solubility and susceptibility to dissolution in high-Mg versus low-Mg calcite [69–72]. However, it should be noted that molluscs have much lower levels of magnesium substitution (less than 4 mol%) than many other organisms, including forams, crustaceans, bryozoans, echinoderms and red corals, which have calcites with levels of up to 45 mol% Mg [71,73]. Indeed, in a study examining shell dissolution under predicted ocean acidification scenarios [47], the lobster cuticle was the most susceptible to dissolution and had a magnesium content at least five times greater than the included bivalve taxa.

By examining the dissolution rate of biomineralized microstructures exposed to a salinity gradient, this study aims to determine the vulnerability of the shells of bivalve taxa to climate change-driven salinity heterogeneity. In this study, we have selected representative microstructures to assess the resilience of the isolated microstructure (*ex situ*) to a broad range of salinities from 0 to 45‰ to make informative comparisons based on the biocomposite itself. Contributory factors to be considered include mineralogy, organic content and crystal size. The following hypotheses are tested: (i) dissolution of microstructures will be greatest at salinities below normal marine conditions (<35‰); (ii) calcite mineralogies will exhibit greater resistance to dissolution than aragonite; and (iii) susceptibility to dissolution will be enhanced in microstructures with low organic content.

2. Material and methods

2.1. Material and microstructure characterization

Six bivalve taxa were selected, representing four key microstructures known to have different proportions of organic content (wt%; calcitic foliae, 0.9 wt% and fibrous prisms, 1.4 wt%; and aragonitic nacre, 3.1–3.4 wt% and crossed lamellar, 2.0–2.1 wt%). Large mature adult specimens were sourced from four habitats (freshwater, coastal lagoon, intertidal and subtidal) and are summarized in table 1. All taxa were collected alive and shell fragments (approximately 1 cm × 1 cm in size) of the selected microstructures obtained using a Dremel tool. Fragments were selected from relatively flat areas of the shell and were obtained from: 20 *Cerastoderma edule*; 20 *Cerastoderma glaucum*; 20 *Mytilus edulis*; 6 *Unio pictorum*; and 3 *Pecten maximus*. Material was selected from taxa with an intact periostracum to avoid areas of previous shell loss and damage. To determine the weight proportion (wt%) of the organic matrix within microstructures, one shell fragment of each taxon was retained (with the periostracum removed by sanding) for thermogravimetric analysis. Fragments were ground using a pestle and mortar, and 10 mg samples were tested using a thermal analyser (Discovery SDT650, TA Instruments at the Department of Materials Science and Metallurgy, University of Cambridge, UK) following the procedure outlined in Telesca *et al.* [38]. Where possible, results of the analysis were cross-checked against the proportions of organic content determined by previous studies to ensure samples were not aberrant [38,47,68]. Crystal width (to the nearest 0.1 µm) and variability (standard

Downloaded from http://royalsocietypublishing.org/rsos/article-pdf/doi/10.1098/rsos.251473/5634029/rsos.251473.pdf
by guest
on 23 January 2026

deviation) were measured from scanning electron micrographs of the exposed shell surfaces in the resin blocks (for details, see below) using ImageJ software. Crystal widths of the crossed lamellar were measured using the same method from scanning electron microscope (SEM) images published in fig. 4 of Milano *et al.* [74] to take advantage of demarcated individual laths.

2.2. Dissolution experiment

Shell fragments were set in individual polyester resin blocks (60 per taxon) so that the flat area of the desired microstructure was parallel to the surface of the resin. Blocks were ground and polished down to a 9 µm grit to expose the shell on the top surface flush with the surface of the resin (figure 1). This process removed any adherent periostracum, existing corrosion or microborings that may have been present on the original surface of the shell. Salinity treatments were prepared to 30 l using Instant Ocean® and deionized water, adjusted manually to the required salinity (± 0.1‰) using a handheld salinity tester (HI-98319, Hanna Instruments). Water pH of the salinity treatments was tested using a pH probe (HQ11D portable meter, Hach, Germany), calibrated using pH buffer solutions of pH 4.01, 7.00 and 10.01. pH values of 8.29, 8.47, 8.38 and 8.12 were recorded for salinities of 10, 20, 35 and 45‰, respectively. Measurements of pH failed to stabilize in the deionized water (0‰). Saturation states of calcite and aragonite at salinities of 10, 20, 35 and 45‰ were calculated using the CO_2SYS program developed by Lewis & Wallis [75]. The respective calcite saturation states were 1.56, 5.46, 10.28 and 9.03, and the aragonite saturation states were 0.88, 3.28, 6.54 and 5.74. Three 10 l replicate tubs with fitted lids to minimize evaporation were prepared for each salinity treatment, making a total of 15 tubs. Each tub was connected to an air pump via silicone tubing and a manifold to maintain water movement at a rate of approximately 5 l min^{-1}. Aquarium check valves were used to prevent water from flowing back into the air tube. Twelve blocks per taxon were exposed to each of the five salinities: 10, 20, 35, 45 and deionized water (0‰). Each salinity treatment had a total of four blocks per taxon in each of the three replicate tubs, with each tub holding a total of 24 blocks. Blocks were oriented with the exposed shell fragment on top (electronic supplementary material, figure S1), and a random number generator was used to randomly place the 24 blocks in each tub. A complete change of water was made every 20 days by mixing up 30 l of each salinity treatment before distributing it into the three replicate 10 l tubs. Salinity was measured every day for the first 14 days of the experiment to ensure stable salinity levels and subsequently monitored weekly. No deviations of more than ±0.1‰ were recorded throughout. The salinity gradient mesocosm was set up at the British Antarctic Survey, Cambridge (electronic supplementary material, figure S2), in a controlled environment room maintained at 10°C and in darkness to help retard the growth of biofilms. Separately, inorganic prisms of aragonite ($n = 15$) and parallelepipeds of calcite ($n = 15$), ranging in weight from 0.15 to 1.33 g, were placed whole (i.e. not embedded in resin) into each tub. We did not embed these inorganic mineral samples because of their tendency to break along their cleavage planes during polishing, which would have had a marked effect on their solubility. Instead, we used these mineral samples to visually compare dissolution patterns between organic and inorganic carbonates. All blocks were removed after 180 days (approx. 6 months).

2.3. Measuring shell thickness loss

Thickness of shell loss (dissolution) was measured using an ultrahigh-definition digital microscope (VHX-7000 Keyence at the Sainsbury's Laboratory, University of Cambridge, UK) that uses high-resolution light-sensitive sensors to visualize and capture surface contours and textures. Serial three-dimensional images of the block surface were stitched to produce a single three-dimensional profile at magnifications of 100×, 400× or 700×, as needed for resolution. Tilt correction of the block was applied using the flat resin margins as reference points. Two-point transects were made across the three-dimensional profile to determine the greatest change in depth (µm) relative to the resin surface. Five transects were made to determine an average amount of dissolution (shell thickness loss). Inorganic blocks were air-dried and weighed to the nearest 0.001 g at the end of the 180 day experiment. The percentage weight loss of each inorganic block was calculated and used to compare levels of dissolution.

2.4. Examining dissolution

From each salinity treatment, one block of each microstructure and the isolated mineral crystals were reserved to characterize the surface textures by SEM (Zeiss EVO HD15 at the Sainsbury's Laboratory,

Downloaded from http://royalsocietypublishing.org/rsos/article-pdf/doi/10.1098/rsos.251473/5634029/rsos.251473.pdf
by guest
on 23 January 2026

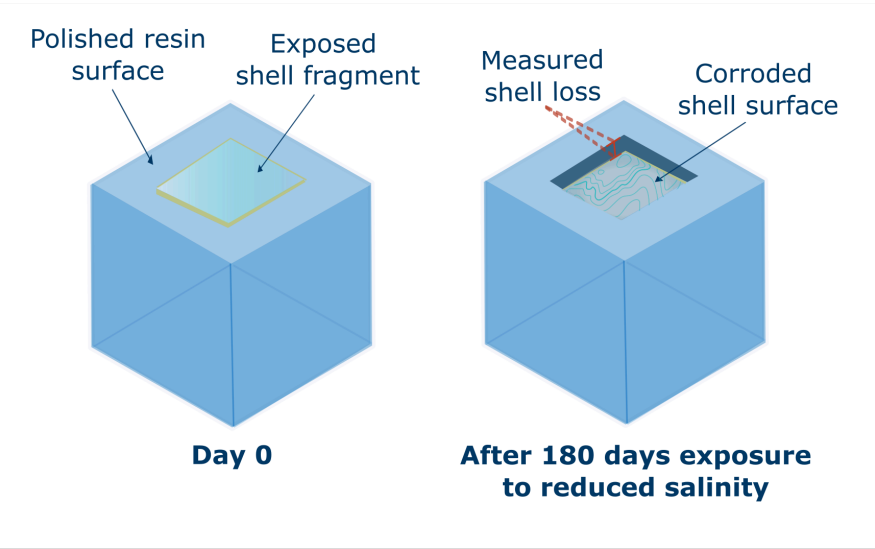

Figure 1. Resin blocks ($n = 60$) exposing shell fragments of six bivalve microstructures were prepared. Blocks were ground to a 9 µm grit to ensure the shell surface was flush with the resin. Blocks were exposed to salinities of 0, 10, 20, 35 and 45‰ for 180 days.

Table 1. Summary of taxon microstructure, habitat and organic content.

mineralogy and microstructure	taxon (*n*)	habitat (salinity)	source of materials	organics (wt%)	crystal size (µm ± s.d.)
calcite; foliae	*Pecten maximus* (king scallop) (3)	subtidal (approx. 35‰)	commercial dealer	0.9	0.9 ± 0.1
calcite; fibrous prisms	*Mytilus edulis* (blue mussel) (15)	intertidal (approx. 35‰)	West Runton, UK	1.4	1.5 ± 0.3
aragonite; nacre	*Mytilus edulis* (blue mussel) (15)	intertidal (approx. 35‰)	West Runton, UK	3.1	4.8 ± 0.5
aragonite; nacre	*Unio pictorum* (freshwater mussel) (6)	freshwater habitat (0‰)	Wicken Fen, UK	3.4	5.3 ± 0.5
aragonite; crossed lamellar	*Cerastoderma edule* (common cockle) (20)	intertidal (approx. 35‰)	Holme-next-to-Sea, UK	2.0	0.6 ± 0.1
aragonite; crossed lamellar	*Cerastoderma glaucum* (lagoon cockle) (20)	coastal lagoon (mean: 17‰)	Slaughden lagoon, UK	2.1	0.6 ± 0.1
inorganic aragonite; crystals	(15)	—	commercial dealer	0	—
inorganic calcite; cleavage rhombs	(15)	—	commercial dealer	0	—

University of Cambridge, UK). Specimens were washed and air-dried before being gold-coated to a thickness of 10 nm and imaged at 20 kV.

2.5. Statistics

Data exploration was carried out following the protocol described in Zuur *et al.* [76]. Shell thickness loss was negligible across microstructures at 35 and 45‰, and to prevent zero inflation and biased parameter estimates, was not included in any analyses [76]. Linear mixed models (LMMs) were applied to determine the influence of shell characteristics on dissolution susceptibility. Variance inflation factors (VIFs) and pairwise scatter plots were used to check for collinearity. VIF values of <3 were considered acceptable. Salinity was included as a categorial factor in all analyses. The *tub* was initially included as a random effect to account for variation among the salinity treatment replicates

Downloaded from http://royalsocietypublishing.org/rsos/article-pdf/doi/10.1098/rsos.251473/5634029/rsos.251473.pdf
by guest
on 23 January 2026

but was subsequently removed for parsimony since the variance was negligible. *Block_ID* was included as a random effect to account for the non-independence of the five shell thickness loss measurements made on each resin block and to avoid pseudoreplication. Model assumptions were validated by plotting residuals versus fitted values, versus each covariate in the model and versus each covariate not in the model. A log transformation was applied to the response variable, shell thickness loss, to meet model assumptions. High collinearity (VIF > 10) between *organics* and *crystal size* (Pearson's r = 0.8) prevented their simultaneous inclusion in mixed model analyses. Instead, they were modelled separately in additive models with *mineralogy* and their interaction with *salinity*. These models were compared using the Akaike information criterion (AIC) and likelihood ratio tests using a baseline model including only *salinity* and *mineralogy*. All analyses were carried out using R (v. 4.4.1). The lme4 [77] package was used to conduct the LMMs, while MuMIn [78] was used to calculate R^2 values, and emmeans [79] was used to back-transform effect sizes, perform pairwise comparisons and discern linear trends.

3. Results

Shell thickness loss was observed in all six of the microstructures at salinities of 0 and 10‰. Three microstructures showed further loss at a salinity of 20‰. Shell thickness loss was negligible at salinities of 35 and 45‰, and the intact shell fragment surfaces revealed by scanning electron micrographs of *C. glaucum* crossed lamellar and *M. edulis* nacre at 35‰ corroborated this (electronic supplementary material, figure S3). The significant variations of shell thickness loss observed across microstructures are demonstrated in figure 2 and highlight the importance of examining the microstructural properties of each taxon.

3.1. Salinity

A strong negative correlation was observed between salinity and shell thickness loss (LMM: $F_{2,176}$ = 249.49, $p < 0.0001$, marginal R^2 = 0.73). Significant levels of shell thickness loss occurred across all microstructures at salinities of 0 and 10‰. Dissolution was discernible at 20‰ in the crossed lamellar and *M. edulis* nacre microstructures, but negligible in the calcite polymorphs and *U. pictorum* nacre (figure 2). Over the 180 days, dissolution was greatest in deionized water (0‰; LMM: estimate = 125.71, 95% CI 107.36–147.20), and decreased significantly with increasing salinity at 10‰ (LMM: estimate = 35.03, 95% CI 29.88–41.06) and 20‰ (LMM: estimate = 5.81, 95% CI 4.65–7.26). There were significant differences in dissolution across microstructures, with some more resistant than others. The general pattern of susceptibility was *C. glaucum* crossed lamellar > *C. edule* crossed lamellar > *M. edulis* nacre > *U. pictorum* nacre > *M. edulis* fibrous prisms > *P. maximus* foliae (LMM: $F_{5,164}$ = 162.47, $p < 0.0001$; figure 2). Divergences from this pattern are described here. There were no significant differences in shell thickness loss between the crossed lamellar microstructures at salinities of 0‰ (LMM: $p > 0.05$, t_{164} = −0.276) and 10‰ (LMM: $p > 0.05$, t_{164} = −0.246), but *C. edule* lost approximately 49.5% less shell thickness than *C. glaucum* at the higher salinity of 20‰ (LMM: $p < 0.0001$, t_{164} = 6.248). No significant difference in shell loss was observed in calcitic microstructures in deionized water (LMM: $p > 0.05$, t_{164} = 1.512), but *P. maximus* lost approximately 41% less shell at a salinity of 10‰ (LMM: $p < 0.0001$, t_{164} = 4.749). At 20‰, there was no significant difference in shell loss between the *C. edule* crossed lamellar and *M. edulis* nacre (LMM: $p > 0.05$, t_{164} = 1.512). No dissolution was discernible in *U. pictorum* nacre at a salinity of 20‰, demonstrating higher resistance to dissolution than the nacre of *M. edulis*.

These results must be considered with the characteristics of the mineralized and organic components outlined above to determine the importance of these factors in driving or retarding shell dissolution. Factors considered in the analyses include mineralogy, organic content and crystal size.

3.2. Mineralogy

Mineralogy was a strong predictor of dissolution susceptibility (LMM: $F_{1,174}$ = 340.4, $p < 0.0001$, marginal R^2 = 0.91). Calcitic microstructures were most resistant to dissolution, losing approximately 50 and 83% less shell thickness than aragonitic microstructures at salinities of 0‰ (LMM: $p < 0.0001$, t_{174} = 7.45) and 10‰ (LMM: $p < 0.0001$, t_{174} = 18.55), respectively.

Downloaded from http://royalsocietypublishing.org/rsos/article-pdf/doi/10.1098/rsos.251473/5634029/rsos.251473.pdf
by guest
on 23 January 2026

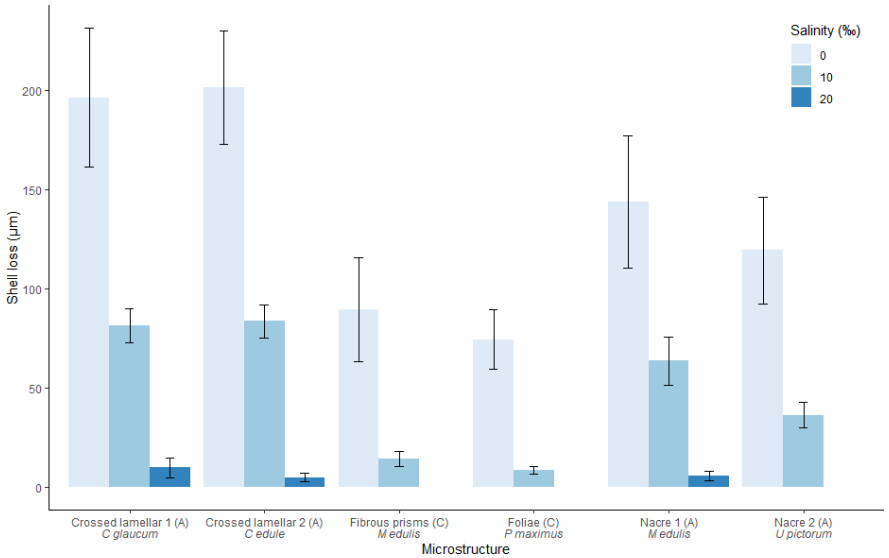

Figure 2. Shell thickness loss measured in microstructures from six bivalve taxa exposed to reduced salinities. Loss of shell was measured in micrometres as the difference between the block and shell surfaces using a high-resolution digital microscope (VHX-7000 Keyence). Error bars represent one standard deviation above and below the mean. A = aragonite; C = calcite.

3.3. Organic matrix and crystal size

Total organic content varied markedly across the different microstructures. Calcitic microstructures exhibited the lowest amounts of organics, with just 0.9 wt% in *P. maximus* foliae and 1.4 wt% in *M. edulis* fibrous prisms. In the aragonitic microstructures, taxa with crossed lamellar microstructures had lower quantities of organics (*C. glaucum*, 2.1 wt%; *C. edule*, 2.0 wt%) compared with nacre (*M. edulis*, 3.1 wt%; *U. pictorum*, 3.4 wt%) (table 1).

Overall, higher proportions of organics improved resistance to dissolution (LMM: $F_{1,172} = 22.57$, $p < 0.0001$), but this relationship varied significantly with salinity (LMM: $F_{1,172} = 20.69$, $p < 0.0001$). Higher organic content was beneficial at the lowest salinity of 0‰ (LMM: slope = −0.59; 95% CI −0.73 to −0.45), but revealed a weakened and nonsignificant influence at salinities of 10‰ (LMM: slope = 0.14, 95% CI −0.28 to −0.00) and 20‰ (LMM: slope = −0.12, 95% CI −0.37 to 0.13).

Increasing crystal size also improved resistance to dissolution significantly (LMM: $F_{1,172} = 27.53$, $p < 0.0001$) and showed a significant interaction with salinity (LMM: $F_{1,172} = 3.46$, $p < 0.05$). Larger crystal size was most advantageous at a salinity of 0‰ (LMM: slope = −0.14; 95% CI −0.19 to −0.10) and showed a weakened effect at a salinity of 10‰ (LMM: slope = −0.07; 95% CI −0.12 to −0.02). The relationship was not significant at a salinity of 20‰ (LMM: slope = −0.05; 95% CI −0.12 to 0.02).

Organic content ($\chi^2 = 63.96$, $p < 0.0001$, AIC = −777.47) and crystal size ($\chi^2 = 39.94$, $p < 0.0001$, AIC = −753.45) significantly improved model fit compared with the baseline (AIC = −719.59). Organic content appeared to have a significantly better fit, and the likelihood ratio chi-square statistic suggested it to be approximately 1.6 times more influential in predicting shell thickness loss than crystal size.

3.4. Surface imaging

SEM imaging revealed the extent of dissolution for each microstructure and variation among them. Organic envelopes did not appear to be retained, suggesting their preferential dissolution before the mineral components. The surface textures observed are characterized by extensive pitting of individual crystals and significant loss of structural integrity at the lowest salinities of 0 and 10‰ (figures 3 and 4). In the crossed lamellar microstructures, individual lamellae were exposed and displayed pronounced irregular and pitted surfaces, resulting in distortion of the usual interdigitation of the first and second orders (figure 3a,b,d,e). Nacre tablets were separated by steep-walled canyons, causing severe loss of integrity. The tablet surfaces were conspicuously perforated, and the margins were ragged (figure 3g,h,j,k). In the fibrillar prisms, dissolution was preferential along the margins of individual prisms, and loss of structural integrity was acute (figure 4a,b). The dissolution extent was modest in microstructures exposed to salinities of 20‰. Individual laths remained highly integrated with little evidence of structural impairment. Only a very small amount of pitting could

Downloaded from http://royalsocietypublishing.org/rsos/article-pdf/doi/10.1098/rsos.251473/5634029/rsos.251473.pdf
by guest
on 23 January 2026

be distinguished (figure 3c,f,i). As the evidence of dissolution was minimal in samples that recorded some loss of shell at 20‰, and the clarity of the individual crystals was much reduced because of uninterrupted interdigitation, microstructures that did not record any amount of shell loss at 20‰ were not imaged by SEM. Scanning electron micrographs of *C. glaucum* crossed lamellar and *M. edulis* nacre at a salinity of 35‰ revealed intact, smooth surfaces that corroborated negligible shell thickness loss and absence of dissolution (electronic supplementary material, figure S3).

The inorganic aragonite and calcite blocks showed similar levels of deterioration as a result of dissolution. Exposure to the lowest salinity (0‰) resulted in obvious and extensive pitting of the aragonite surfaces, with a pronounced irregular texture and preferential loss of material along parallel lines that reflect the cleavage planes (figure 5a). Although pitting was less obvious in the inorganic aragonite blocks exposed to a salinity of 10‰, there was significant deterioration along the crystal edges (figure 5b). The effects of dissolution appeared less severe on the inorganic calcite rhombs, with patches of roughness observed across the surface. With no obvious pitting, dissolution was preferential along cleavages at the lowest salinities (0 and 10‰), resulting in some structural deterioration (figure 5c,d).

4. Discussion

This study of isolated bivalve microstructures has allowed a first-order examination of shell dissolution across a salinity gradient. Our findings support our initial hypotheses and reveal: (i) the high susceptibility of bivalve calcium carbonate shells to dissolution in salinities below normal marine conditions of 35‰, with the rate of dissolution increasing significantly and progressively with decreasing salinity; (ii) that calcite polymorphs show significantly more resistance to low-salinity conditions than aragonite, with mineralogy the best predictor for dissolution; and (iii) that organic content has an important influence on the dissolution of aragonitic microstructures.

4.1. Corrosive potential of low salinity

While ocean acidification and its deleterious effects on calcareous skeletons have been well studied, the corrosive potential of ocean freshening is of increasing concern, as we experience more severe precipitation events, especially at high latitudes with accelerated melting of the cryosphere. In marine environments, changes in the hydrological cycle are largely reflected by shifts in salinity [20,21]. Desalinization is most severe along coastlines where there are significant levels of freshwater input via river flooding and ice melt. The decreasing calcium carbonate saturation state and concentrations of calcification substrates along the salinity gradient create challenging conditions for calcifying marine organisms [3,28,29]. The amounts of shell thickness loss revealed in this study were significant and are comparable with the findings of a study investigating dissolution under future ocean acidification conditions carried out by Chadwick *et al.* [47]. The authors used a technique outlined in Kennish & Lutz [80] to manually measure shell thickness loss and found a reduction of less than 25 µm in the shell thickness of the crossed lamellar microstructure after 100 days of exposure to the predicted end-century pH of 7.65. Coastal salinity regimes show increasing seasonal variability with a changing climate, reflected by greater ranging fluctuations from low salinity, driven by higher levels of precipitation in winter, to increasingly hypersaline conditions, driven by increasing summer temperatures and rates of evaporation [22,23]. So, although periods at extreme salinities are impermanent, the ranges of fluctuation are likely increasing under ongoing climate change and will reflect oscillating periods of more intense dissolution and impediment to shell building in the natural environment. These effects will be most significant in marginal seas and isolated environments like coastal lagoons. Late twenty-first century (2070–2100) predictions indicate salinity reductions of 29–45% in the already low-salinity Baltic Sea (average salinity of 7‰), driven by increased river flow and changes in precipitation–evaporation dynamics [81,82]. Similarly, significant and severe salinity drops in the Rías Baixas, Spain, are predicted with forecasted extreme precipitation events [83]. In the Antarctic intertidal, organisms are already experiencing salinities as low as 12‰, with more pronounced effects on organisms directly exposed to melt streams due to freshwater runoff [84]. The findings of this study demonstrate the deleterious potential ocean freshening may have on the integrity of marine invertebrate skeletons, especially in nearshore areas.

Downloaded from http://royalsocietypublishing.org/rsos/article-pdf/doi/10.1098/rsos.251473/5634029/rsos.251473.pdf
by guest
on 23 January 2026

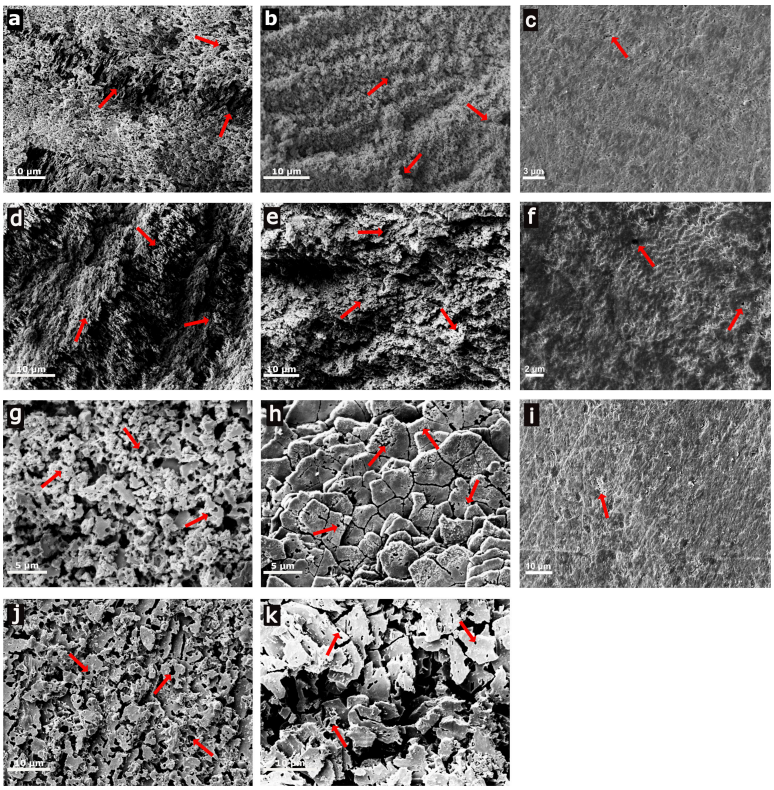

Figure 3. Scanning electron micrographs of aragonitic microstructures after exposure to salinities of (a,d,g,j) 0‰, (b,e,h,k) 10‰ and (c,f,i) 20‰ for 180 days. Crossed lamellar of (a–c) *Cerastoderma glaucum* and (d–f) *C. edule*; nacre of (g–i) *Mytilus edulis* and (j,k) *Unio pictorum*. Pitting of individual crystals and structural damage demonstrate the extent of dissolution (arrows).

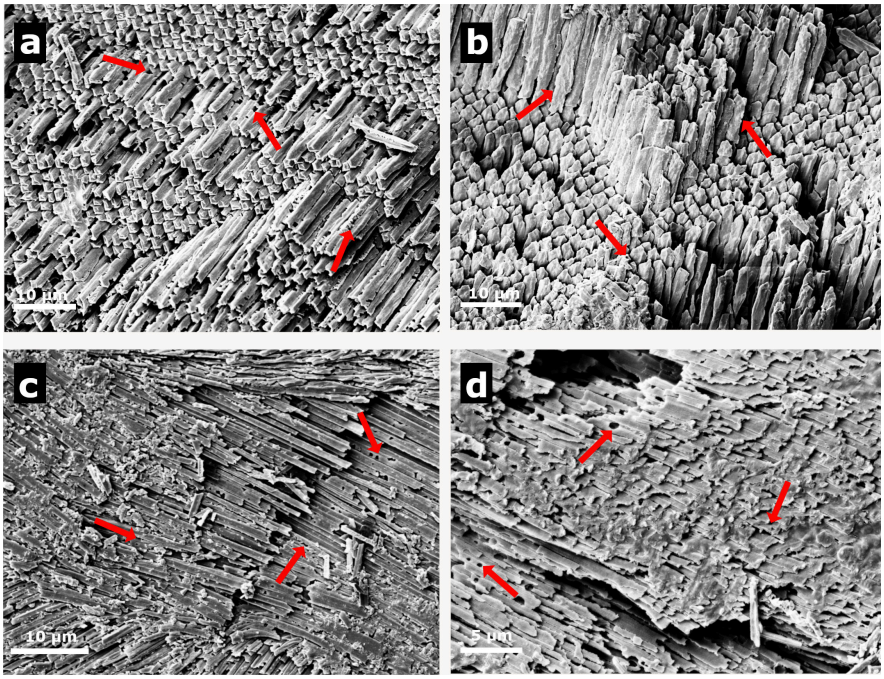

Figure 4. Scanning electron micrographs of calcitic microstructures after exposure to salinities of (a,c) 0‰ and (b,d) 10‰ for 180 days. (a,b) Fibrous prisms of *Mytilus edulis* and (c,d) foliae of *Pecten maximus*. Pitting of individual crystals and structural damage demonstrate the extent of dissolution (arrows).

Downloaded from http://royalsocietypublishing.org/rsos/article-pdf/doi/10.1098/rsos.251473/5634029/rsos.251473.pdf
by guest
on 23 January 2026

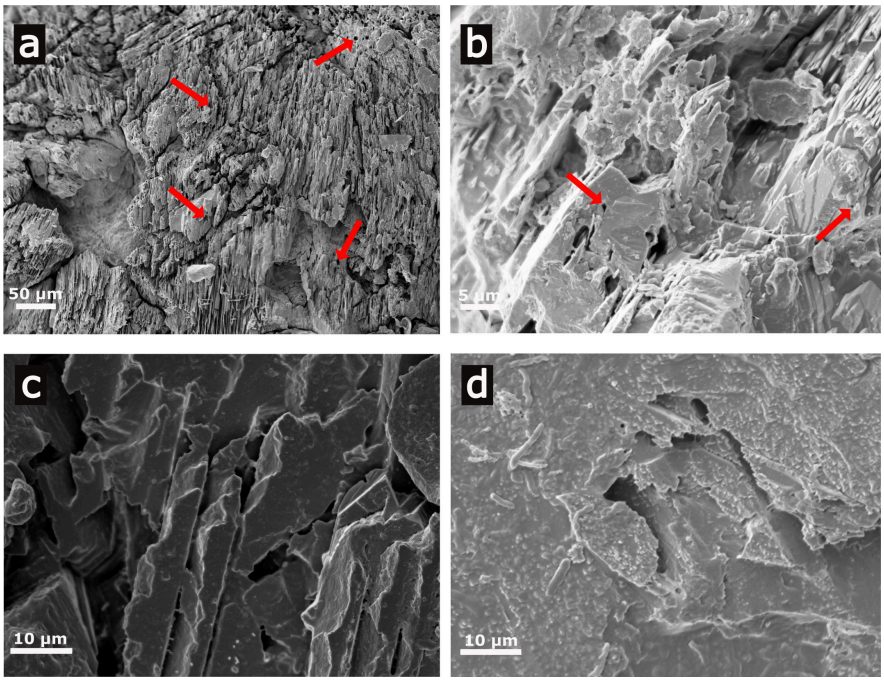

Figure 5. Scanning electron micrographs of inorganic (a,b) aragonite and (c,d) calcite blocks after exposure to salinities of (a,c) 0‰ and (b,d) 10‰ for 180 days. (a,b) Pitting of individual inorganic aragonite crystals and structural damage demonstrate the extent of dissolution (arrows). (c,d) Dissolution is preferential along the cleavages of the inorganic calcite, with patches of irregular surface texture.

4.2. Microstructural characteristics

4.2.1. Mineralogy as a predictor for dissolution

All shelled molluscs secrete an organic periostracum coating on the external shell surface, which provides support for calcium carbonate deposition, but also functions to protect the mineral components from dissolution [32]. Many taxa inhabiting adverse environments, e.g. fresh or acidic waters, have evolved especially thick periostraca [31,85]. However, the protection of the periostracum is limited by its stochastic deterioration or abrasion, which depends on many factors, including the surrounding environment and substrate, damage caused by grazers and predators and, of course, the thickness of the periostracum produced by a particular taxon. This is especially problematic for long-lived taxa, particularly on the oldest parts of the shell at the umbo, where exposure has been longest. Once the periostracum has been lost, it cannot be restored and results in the exposure of the calcareous shell beneath to dissolution [33]. SEM images of a two-year-old *C. glaucum* enduring low salinity (7–8‰) conditions in the Baltic Sea show extensive shell dissolution after the complete loss of periostracum at the umbo and even towards the ventral margins (figure 6). Understanding the capacity of carbonate shell layers to resist dissolution in corrosive low-salinity conditions is critical to inform predictions on the resilience of species to climate-driven salinity heterogeneity.

Although inorganic calcite is 35% less soluble than inorganic aragonite [66], many other factors may also influence the solubility of different shell microstructures, such as organic content, crystal size and morphology [47,62]. In this study, mineralogy was an important predictor for dissolution, explaining 91.0% of the variability at salinities of 0, 10 and 20‰, and 1.6 times more influential than crystal size. Calcite is thought to be energetically less costly to build than aragonite [3], which may prove a further advantage, allowing for an increased reserve of energy for other biological processes in an already physiologically stressful environment. Indeed, *M. edulis* precipitates an increasing proportion of calcite relative to aragonite in its bimineralic shell along decreasing salinity gradients [38,53]. It remains intriguing as to why no freshwater molluscs have evolved to secrete a calcitic outermost layer, despite multiple invasions into these habitats [62].

Downloaded from http://royalsocietypublishing.org/rsos/article-pdf/doi/10.1098/rsos.251473/5634029/rsos.251473.pdf
by guest
on 23 January 2026

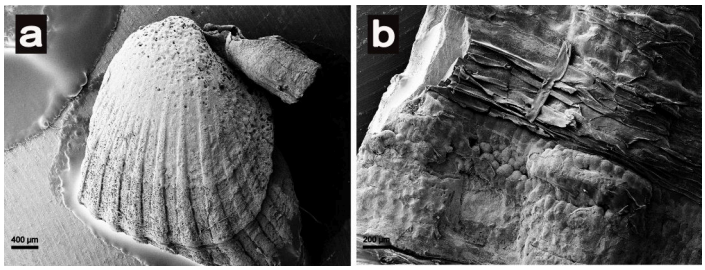

Figure 6. SEM micrographs of a two-year-old *Cerastoderma glaucum* specimen collected alive from the Baltic Sea, where it endures low salinities of around 7–8‰. (a) Periostracum is completely absent at the umbo, inviting extensive dissolution of the mineral layer and considerable structural damage. (b) Periostracum can be seen peeling away towards the ventral margin, with areas of distinct pitting obvious across the unprotected aragonitic layer.

4.2.2. Function of the organic matrix

The role of the organic matrix within a molluscan shell is difficult to determine. The organic matrix itself is a complex mixture of components (proteins, polysaccharides and chitin) and occurs in taxon- and microstructure-specific proportions both between and within crystal units (see reviews by [39,60,86]). Organic components can be separated into two fractions based on their solubility in aqueous solutions. The soluble fraction is characterized by hydrophilic proteins rich in aspartic acid, while the insoluble fraction is characterized by hydrophobic glycine- or alanine-rich proteins derived from silk fibroins and a framework of the polysaccharide β-chitin [87–90]. Doubtless, the different organic components have multiple functions, for example, determining the expressed polymorph or microstructure [39,64], or controlling biomechanical properties (e.g. [35]). It also seems likely that the organic matrix plays a role in maintaining shell integrity, but its complexity has led to contrary findings. The presence of organic membranes within the shell may protect crystallites from dissolution [35,38,91,92], or serve as a microbial substratum in nonsterile conditions, leading to its decay, subsequent dissociation of crystals and eventual disintegration of the shell [68]. In this study, we have revealed organic content to be critical in retarding the dissolution of biogenic calcium carbonate shells.

The aragonitic microstructures investigated in this study fall into two categories: organic rich and organic poor. The organic-rich nacre (*U. pictorum* and *M. edulis*) consists of thin, small (4.8–5.3 µm) nacre tablets. Each individual tablet is surrounded by an organic envelope [93], providing flexibility in life, but also protecting individual tablets from dissolution. The organic-rich nacre of *U. pictorum* and *M. edulis* was distinctly more resistant to dissolution than the organic-poor crossed lamellar microstructures, losing significantly less shell at the lowest salinities. Remarkably, *U. pictorum* also measured negligible loss of shell at a salinity of 20‰, as did the more resistant calcite mineralogies. Meanwhile, the organic-poor crossed lamellar microstructures lack obvious shrouding material among the third-order lamellae, and the use of transmission electron microscopy is required to detect the thin membranes that are 30 nm thick [68,94,95]. Comparing the two calcitic microstructures, the fibrous prisms of mytilids have clear organic sheaths around 40 nm thick between adjacent prisms [96], while the foliated *P. maximus* layers are defined by much finer organic membranes [97]. The high energetic costs of synthesizing higher proportions of organic matrix are likely not as beneficial in the calcite polymorphs, which are already more microstructurally resilient to dissolution [98].

Our results differ from the increased susceptibility of organic-enriched microstructures to dissolution in acidic seawater observed by Chadwick *et al.* [47], but this probably reflects differences in the microbial decay of the organics. Despite partially sterilizing the natural seawater to reduce microbial activity, Chadwick *et al.* [47] described the growth of biofilms and endolithic algae that is likely to have promoted the dissolution of the organic material. Destruction of the organic matrix by microbial decomposition is therefore likely to further exacerbate dissolution in natural conditions throughout the shelled organism's lifetime [67,68]. This primary loss of the binding matrix may disrupt the microstructural scaffold, loosening crystallites and accelerating dissolution as the reactive surface area increases [67,68]. In our experiment, we specifically chose to minimize microbial activity. We used artificial seawater prepared with deionized water and set the experiment up in a controlled environment room at a constant temperature of 10°C, in the dark. No biofilms were observed on individual blocks, and SEM imaging confirmed the absence of endolith boreholes on any microstructure. Given the extent of microboring observed by Glover & Kidwell [68] in bivalve shells after two weeks of exposure in nonsterile seawater, we are confident that our results are not influenced by microbial activity.

Downloaded from http://royalsocietypublishing.org/rsos/article-pdf/doi/10.1098/rsos.251473/5634029/rsos.251473.pdf
by guest
on 23 January 2026

A further factor that might be considered is the isomorphic substitution of Mg^{2+} for Ca^{2+} in the calcium carbonate. While aragonite does not easily tolerate the incorporation of small Mg^{2+} ions, its substitution in calcite can increase its thermodynamic solubility [70,72]. High biogenic Mg-calcites are considered to have Mg : Ca ratios of more than 0.03 [99], several factors higher than the concentrations of Mg^{2+} incorporated into *P. maximus* (0.0055) and *M. edulis* (0.0021), values recorded by Chadwick *et al.* [47]. So, although *P. maximus* exhibits a concentration of Mg^{2+} twice that of *M. edulis*, the levels are probably not enough to influence the chemical behaviour of the biogenic calcite in our experiments.

It should be noted that there is potential for organisms to mitigate dissolution by inducing compensatory mechanisms, including the production of thicker, more protective shells [37,48] or periostraca [38,43,85]. Increased proportions of organic content have also been observed to improve chemical resistance to dissolution in *Crassostrea virginica* [35] and *Mytilus edulis* [38]. Such adaptations, however, often come at the cost of trade-offs. For example, the improved chemical resistance of organic-enriched *Crassostrea virginica* to low-salinity dissolution comes at the cost of an overall more brittle shell of reduced shell thickness [35]. Furthermore, the costs of calcification in low salinity can significantly limit shell growth and size [29,100], which may have significant effects on predator–prey relationships.

5. Conclusion

This study reveals the increasing vulnerability of bivalve calcium carbonate shells to dissolution at salinities below normal marine conditions. Aragonitic polymorphs are significantly more at risk than calcitic ones, particularly in microstructures with lower proportions of organic matrix. However, the limited sample size of this study meant that several factors (organic content, Mg : Ca ratio, crystal size) could not be conclusively considered, particularly in the calcite polymorphs. It would be useful for future research to explore a broader variety of taxa and microstructures to allow a more comprehensive understanding of the susceptibility of biomineralized skeletons to dissolution in low salinities. Investigating the impact of hypersaline conditions on calcification is also important as lower latitudes experience more intense warming and frequent periods of drought, resulting in increased salinity in many lagoonal systems.

Climate change-driven ocean freshening is likely to have significant impacts on the integrity of biogenic calcium carbonate shells. Even the most resistant taxa with shells of calcite mineralogy are vulnerable to significant amounts of shell loss at low salinities. As a first-order examination, this study excluded other stressors, such as ocean acidification and warming, and was performed under sterile conditions. Although these results may therefore provide a conservative representation of the abiotic potential for dissolution, the biological capacity of living organisms to employ compensatory mechanisms to counteract dissolution is not evaluated. The implications of dissolution on shell material *ex situ* should therefore be extrapolated with care into the complex and multifactorial natural environment. While some species have evolved compensatory mechanisms to tolerate brackish and even freshwater habitats, taxa lacking such adaptations may not respond readily to the rapid shifts in salinity experienced following intense precipitation events or future large-scale ice melt in polar regions. These challenges are further amplified by the energetic and physiological demands of low salinity, which may also impact the capacity of species to biomineralize effectively [101,102]. Freshwater invertebrates may already be well adapted to corrosive undersaturated calcium carbonate conditions, but enhanced water current velocities following storm and flooding events can also significantly impact the dissolution rate of biomineralized exoskeletons [44]. Future predictions indicate further intensification of the hydrological cycle with continued global warming. Vital to survival, reduced integrity of bivalve shells could have far-reaching implications on ecosystem function and predator–prey interactions.

Ethics. This work did not require ethical approval from a human subject or animal welfare committee.

Data accessibility. Data and relevant code for this research work are stored in GitHub: https://github.com/bethanyfrancesking/Salinity_Dissolution and have been archived within the Zenodo repository [103].

Electronic supplementary material is available online [104].

Declaration of AI use. We have not used AI-assisted technologies in creating this article.

Authors' contributions. B.F.K.: conceptualization, data curation, formal analysis, investigation, methodology, project administration, visualization, writing—original draft, writing—review and editing; L.S.P.: conceptualization, methodology, supervision, writing—review and editing; E.M.H.: conceptualization, methodology, supervision, writing—review and editing.

Downloaded from http://royalsocietypublishing.org/rsos/article-pdf/doi/10.1098/rsos.251473/5634029/rsos.251473.pdf
by guest
on 23 January 2026

All authors gave final approval for publication and agreed to be held accountable for the work performed therein.

Conflict of interest declaration. We declare we have no competing interests.

Funding. B.F.K. was supported by the Vice-Chancellor's, Newnham College & Earth Sciences Scholarship at the University of Cambridge.

Acknowledgements. We thank Gareth Evans and Raymond Wightman for providing specialist assistance with imaging technologies, Antonio Checa for his guidance on microstructural properties and the relevant literature, and Sam Kentwell, Rebecca Smith and Guy Hillyard for assistance in setting up and maintenance of experimental regimes. We would also like to thank the three anonymous reviewers for their valuable comments.

References

1. Podbielski I, Hiebenthal C, Hajati MC, Bock C, Bleich M, Melzner F. 2022 Capacity for cellular osmoregulation defines critical salinity of marine invertebrates at low salinity. *Front. Mar. Sci*. **9**, 898364. (doi:10.3389/fmars.2022.898364)
2. Wikner J, Andersson A. 2012 Increased freshwater discharge shifts the trophic balance in the coastal zone of the northern Baltic Sea. *Glob. Chang. Biol*. **18**, 2509–2519. (doi:10.1111/j.1365-2486.2012.02718.x)
3. Thomsen J, Ramesh K, Sanders T, Bleich M, Melzner F. 2018 Calcification in a marginal sea—influence of seawater [Ca^{2+}] and carbonate chemistry on bivalve shell formation. *Biogeosciences* **15**, 1469–1482. (doi:10.5194/bg-15-1469-2018)
4. Smyth K, Elliott M. 2016 Effects of changing salinity on the ecology of the marine environment. In *Stressors in the marine environment: physiological and ecological responses; societal implications* (eds M Solan, N Whiteley), pp. 161–174. Oxford, UK: Oxford University Press. (doi:10.1093/acprof:oso/9780198718826.003.0009)
5. Asadieh B, Krakauer NY. 2015 Global trends in extreme precipitation: climate models versus observations. *Hydrol. Earth Syst. Sci*. **19**, 877–891. (doi:10.5194/hess-19-877-2015)
6. Kharin VV, Zwiers FW, Zhang X, Wehner M. 2013 Changes in temperature and precipitation extremes in the CMIP5 ensemble. *Clim. Chang*. **119**, 345–357. (doi:10.1007/s10584-013-0705-8)
7. Röthig T, Trevathan-Tackett SM, Voolstra CR, Ross C, Chaffron S, Durack PJ, Warmuth LM, Sweet M. 2023 Human-induced salinity changes impact marine organisms and ecosystems. *Glob. Chang. Biol*. **29**, 4731–4749. (doi:10.1111/gcb.16859)
8. Hanlon HM, Bernie D, Carigi G, Lowe JA. 2021 Future changes to high impact weather in the UK. *Clim. Chang*. **166**, 50. (doi:10.1007/s10584-021-03100-5)
9. Cardoso PG, Raffaelli D, Lillebø AI, Verdelhos T, Pardal MA. 2008 The impact of extreme flooding events and anthropogenic stressors on the macrobenthic communities' dynamics. *Estuar. Coast. Shelf Sci*. **76**, 553–565. (doi:10.1016/j.ecss.2007.07.026)
10. Peteiro LG, Woodin SA, Wethey DS, Costas-Costas D, Martínez-Casal A, Olabarria C, Vázquez E. 2018 Responses to salinity stress in bivalves: evidence of ontogenetic changes in energetic physiology on *Cerastoderma edule*. *Sci. Rep*. **8**, 8329. (doi:10.1038/s41598-018-26706-9)
11. Barrett NJ, Harper EM, Peck LS. 2025 Evaluating the acclimation capacity of two keystone Antarctic echinoderms to coastal freshening. *Sci. Total Environ*. **968**, 178895. (doi:10.1016/j.scitotenv.2025.178895)
12. McKnight E, Spake R, Bates A, Smale DA, Rius M. 2021 Non-native species outperform natives in coastal marine ecosystems subjected to warming and freshening events. *Glob. Ecol. Biogeogr*. **30**, 1698–1712. (doi:10.1111/geb.13318)
13. Barnes RSK. 1991 Dilemmas in the theory and practice of biological conservation as exemplified by British coastal lagoons. *Biol. Conserv*. **55**, 315–328. (doi:10.1016/0006-3207(91)90035-8)
14. Bamber RN, Batten SD, Sheader M, Bridgwater ND. 1992 On the ecology of brackish water lagoons in Great Britain. *Aquat. Conserv. Mar. Freshw. Ecosyst*. **2**, 65–94. (doi:10.1002/aqc.3270020105)
15. Minx JC *et al*. 2021 A comprehensive and synthetic dataset for global, regional, and national greenhouse gas emissions by sector 1970–2018 with an extension to 2019. *Earth Syst. Sci. Data* **13**, 5213–5252. (doi:10.5194/essd-13-5213-2021)
16. Calvin K, Dasgupta D, Krinner G, Mukherji A, Thorne PW, Trisos C. 2023 Climate change 2023: synthesis report. In *Contribution of working groups I, II and III to the sixth assessment report of the Intergovernmental Panel on Climate Change* (eds Core Writing Team, H Lee, J Romero). Geneva, Switzerland: Intergovernmental Panel on Climate Change (IPCC). (doi:10.59327/IPCC/AR6-9789291691647)
17. Liu B, Tan X, Gan TY, Chen X, Lin K, Lu M, Liu Z. 2020 Global atmospheric moisture transport associated with precipitation extremes: mechanisms and climate change impacts. *WIREs Water* **7**, e1412. (doi:10.1002/wat2.1412)
18. Semmler T, Jacob D. 2004 Modeling extreme precipitation events—a climate change simulation for Europe. *Glob. Planet. Chang*. **44**, 119–127. (doi:10.1016/j.gloplacha.2004.06.008)
19. Trenberth K. 2011 Changes in precipitation with climate change. *Clim. Res*. **47**, 123–138. (doi:10.3354/cr00953)
20. Durack P. 2015 Ocean salinity and the global water cycle. *Oceanography* **28**, 20–31. (doi:10.5670/oceanog.2015.03)
21. Durack PJ, Wijffels SE. 2010 Fifty-year trends in global ocean salinities and their relationship to broad-scale warming. *J. Clim*. **23**, 4342–4362. (doi:10.1175/2010jcli3377.1)
22. Douville H, Cheng L. 2024 Asymmetric sea surface salinity response to global warming: 'Fresh gets fresher but salty hesitates'. *Geophys. Res. Lett*. **51**, e2023GL107944. (doi:10.1029/2023GL107944)

Downloaded from http://royalsocietypublishing.org/rsos/article-pdf/doi/10.1098/rsos.251473/5634029/rsos.251473.pdf
by guest
on 23 January 2026

23. Durack PJ, Wijffels SE, Matear RJ. 2012 Ocean salinities reveal strong global water cycle intensification during 1950 to 2000. *Science* **336**, 455–458. (doi:10.1126/science.1212222)
24. Haumann FA, Gruber N, Münnich M, Frenger I, Kern S. 2016 Sea-ice transport driving Southern Ocean salinity and its recent trends. *Nature* **537**, 89–92. (doi:10.1038/nature19101)
25. Li H, Fedorov AV. 2021 Persistent freshening of the Arctic Ocean and changes in the North Atlantic salinity caused by Arctic sea ice decline. *Clim. Dyn.* **57**, 2995–3013. (doi:10.1007/s00382-021-05850-5)
26. Wunderling N, Willeit M, Donges JF, Winkelmann R. 2020 Global warming due to loss of large ice masses and Arctic summer sea ice. *Nat. Commun*. **11**, 5177. (doi:10.1038/s41467-020-18934-3)
27. Gosling EM. 2003 *Bivalve molluscs: biology, ecology, and culture*. Oxford, UK: Fishing News Books.
28. Sanders T, Thomsen J, Müller JD, Rehder G, Melzner F. 2021 Decoupling salinity and carbonate chemistry: low calcium ion concentration rather than salinity limits calcification in Baltic Sea mussels. *Biogeosciences* **18**, 2573–2590. (doi:10.5194/bg-18-2573-2021)
29. Sanders T, Schmittmann L, Nascimento-Schulze JC, Melzner F. 2018 High calcification costs limit mussel growth at low salinity. *Front. Mar. Sci*. **5**, 352. (doi:10.3389/fmars.2018.00352)
30. Ries JB, Ghazaleh MN, Connolly B, Westfield I, Castillo KD. 2016 Impacts of seawater saturation state ($\Omega A = 0.4–4.6$) and temperature (10, 25°C) on the dissolution kinetics of whole-shell biogenic carbonates. *Geochim. Cosmochim. Acta* **192**, 318–337. (doi:10.1016/j.gca.2016.07.001)
31. Harper EM. 1997 The molluscan periostracum: an important constraint in bivalve evolution. *Palaeontology* **40**, 71–97. (doi:10.5281/zenodo.16670830)
32. Taylor JD, Kennedy WJ. 1969 The influence of the periostracum on the shell structure of bivalve molluscs. *Calcif. Tissue Res*. **3**, 274–283. (doi:10.1007/bf02058669)
33. Peck VL, Tarling GA, Manno C, Harper EM, Tynan E. 2016 Outer organic layer and internal repair mechanism protects pteropod *Limacina helicina* from ocean acidification. *Deep Sea Res. II Top. Stud. Oceanogr.* **127**, 41–52. (doi:10.1016/j.dsr2.2015.12.005)
34. Telesca L, Michalek K, Sanders T, Peck LS, Thyrring J, Harper EM. 2018 Blue mussel shell shape plasticity and natural environments: a quantitative approach. *Sci. Rep*. **8**, 2865. (doi:10.1038/s41598-018-20122-9)
35. Telesca L, Linsley BK, Witek L, Hönisch B. 2024 Biomineralization and biomechanical trade-offs under heterogeneous environments in the eastern oyster *Crassostrea virginica*. *J. Molluscan Stud*. **90**, eyae033. (doi:10.1093/mollus/eyae033)
36. Westerbom M, Kilpi M, Mustonen O. 2002 Blue mussels, *Mytilus edulis*, at the edge of the range: population structure, growth and biomass along a salinity gradient in the north-eastern Baltic Sea. *Mar. Biol*. **140**, 991–999. (doi:10.1007/s00227-001-0765-6)
37. Telesca L, Peck LS, Backeljau T, Heinig MF, Harper EM. 2020 A century of coping with environmental and ecological changes via compensatory biomineralization in mussels. *Glob. Chang. Biol.* **27**, 624–639. (doi:10.1111/gcb.15417)
38. Telesca L, Peck LS, Sanders T, Thyrring J, Sejr MK, Harper EM. 2019 Biomineralization plasticity and environmental heterogeneity predict geographical resilience patterns of foundation species to future change. *Glob. Chang. Biol*. **25**, 4179–4193. (doi:10.1111/gcb.14758)
39. Clark MS. 2020 Molecular mechanisms of biomineralization in marine invertebrates. *J. Exp. Biol*. **223**, b206961. (doi:10.1242/jeb.206961)
40. Fitzer SC, Torres Gabarda S, Daly L, Hughes B, Dove M, O'Connor W, Potts J, Scanes P, Byrne M. 2018 Coastal acidification impacts on shell mineral structure of bivalve mollusks. *Ecol. Evol*. **8**, 8973–8984. (doi:10.1002/ece3.4416)
41. Araujo R, Delvene G, Munt M. 2014 Presence of organic layers in shells of fossil and recent Unionoida (Bivalvia) and their implications. *J. Molluscan Stud*. **80**, 74–83. (doi:10.1093/mollus/eyt048)
42. Harper EM. 1994 Are conchiolin sheets in corbulid bivalves primarily defensive? *Palaeontology* **37**, 551–578.
43. Marshall DJ, Tsikouras B. 2023 Clay-shielded estuarine gastropods are better protected against environmental acidification than unshielded individuals. *Sci. Total Environ*. **866**, 161367. (doi:10.1016/j.scitotenv.2022.161367)
44. Ilarri MI, Souza AT, Sousa R. 2015 Contrasting decay rates of freshwater bivalves' shells: aquatic versus terrestrial habitats. *Limnologica* **51**, 8–14. (doi:10.1016/j.limno.2014.10.002)
45. Isaji S. 1993 Formation of organic sheets in the inner shell layer of *Geloina* (Bivalvia: Corbiculidae): an adaptive response to shell dissolution. *Veliger* **36**, 166–173.
46. Isaji S. 1995 Defensive strategies against shell dissolution in bivalves inhabiting acidic environments: the case of *Geloina* (Corbiculidae) in mangrove swamps. *Veliger* **38**, 235–246.
47. Chadwick M, Harper EM, Lemasson A, Spicer JI, Peck LS. 2019 Quantifying susceptibility of marine invertebrate biocomposites to dissolution in reduced pH. *R. Soc. Open Sci*. **6**, 190252. (doi:10.1098/rsos.190252)
48. Cross EL, Harper EM, Peck LS. 2019 Thicker shells compensate extensive dissolution in brachiopods under future ocean acidification. *Environ. Sci. Technol*. **53**, 5016–5026. (doi:10.1021/acs.est.9b00714)
49. Marshall D, Aminuddin A, Mustapha N, Wah DTT, De Silva L. 2018 Gastropod shell dissolution as a tool for biomonitoring marine acidification, with reference to coastal geochemical discharge. *Preprints* 2018030022. (doi:10.20944/preprints201803.0022.v1)
50. Marshall DJ, Tsikouras B. 2024 Compensatory shell thickening in corrosive environments varies between related rocky-shore and estuarine gastropods. *Mar. Environ. Res*. **198**, 106536. (doi:10.1016/j.marenvres.2024.106536)
51. Peck VL, Oakes RL, Harper EM, Manno C, Tarling GA. 2018 Pteropods counter mechanical damage and dissolution through extensive shell repair. *Nat. Commun*. **9**, 264. (doi:10.1038/s41467-017-02692-w)

Downloaded from http://royalsocietypublishing.org/rsos/article-pdf/doi/10.1098/rsos.251473/5634029/rsos.251473.pdf
by guest
on 23 January 2026

52. Waldbusser GG, Hales B, Langdon CJ, Haley BA, Schrader P, Brunner EL, Gray MW, Miller CA, Gimenez I. 2015 Saturation-state sensitivity of marine bivalve larvae to ocean acidification. *Nat. Clim. Chang*. **5**, 273–280. (doi:10.1038/nclimate2479)
53. Piwoni-Piórewicz A, Strekopytov S, Humphreys-Williams E, Najorka J, Szymczycha B, Kukliński P. 2022 Polymorphism of $CaCO_3$ and the variability of elemental composition of the calcareous skeletons secreted by invertebrates along the salinity gradient of the Baltic Sea. *Geobiology* **20**, 575–596. (doi:10.1111/gbi.12496)
54. Kruft Welton RA, Hoppit G, Schmidt DN, Witts JD, Moon BC. 2024 Reviews and syntheses: the clam before the storm—a meta-analysis showing the effect of combined climate change stressors on bivalves. *Biogeosciences* **21**, 223–239. (doi:10.5194/bg-21-223-2024)
55. Gutiérrez JL, Jones CG, Strayer DL, Iribarne OO. 2003 Mollusks as ecosystem engineers: the role of shell production in aquatic habitats. *Oikos* **101**, 79–90. (doi:10.1034/j.1600-0706.2003.12322.x)
56. FAO. 2016 *The state of world fisheries and aquaculture 2016. Contributing to food security and nutrition for all*. Rome, Italy: FAO.
57. Verdelhos T, Veríssimo H, Marques JC, Anastácio P. 2021 Behavioural responses of *Cerastoderma edule* as indicators of potential survival strategies in the face of flooding events. *Appl. Sci*. **11**, 6436. (doi:10.3390/app11146436)
58. Parada JM, Molares J, Otero X. 2012 Multispecies mortality patterns of commercial bivalves in relation to estuarine salinity fluctuation. *Estuaries Coasts* **35**, 132–142. (doi:10.1007/s12237-011-9426-2)
59. Stanley SM. 1970 *Relation of shell form to life habits of the Bivalvia (Mollusca)*. Boulder, CO: Geological Society of America. (doi:10.1130/MEM125)
60. Checa AG. 2018 Physical and biological determinants of the fabrication of molluscan shell microstructures. *Front. Mar. Sci*. **5**, 353. (doi:10.3389/fmars.2018.00353)
61. Taylor JD, Kennedy WJ, Hall A. 1969 The Shell Structure and Mineralogy of the Bivalvia Introduction. Nuculacea—Trigonacea. *Bulletin of the British Museum (Natural History). Zoology.* **Supplement 3**, 1–125. (doi:10.5962/p.312694)
62. Harper EM. 2000 Are calcitic layers an effective adaptation against shell dissolution in the Bivalvia? *J. Zool.* **251**, 179–186. (doi:10.1111/j.1469-7998.2000.tb00602.x)
63. Taylor JD, Layman M. 1972 The mechanical properties of bivalve (Mollusca) shell structures. *Palaeontology* **15**, 73–87. (doi:10.5281/zenodo.16241285)
64. Checa AG, Macías-Sánchez E, Harper EM, Cartwright JHE. 2016 Organic membranes determine the pattern of the columnar prismatic layer of mollusc shells. *Proc. R. Soc. B* **283**, 20160032. (doi:10.1098/rspb.2016.0032)
65. Harper EM, Checa AG. 2020 Tightly shut: flexible valve margins and microstructural asymmetry in pterioid bivalves. *Mar. Biol*. **167**, 78. (doi:10.1007/s00227-020-03693-y)
66. Mucci A. 1983 The solubility of calcite and aragonite in seawater at various salinities, temperatures, and one atmosphere total pressure. *Am. J. Sci*. **283**, 780–799. (doi:10.2475/ajs.283.7.780)
67. Peck LS, Clark MS, Power D, Reis J, Batista FM, Harper EM. 2015 Acidification effects on biofouling communities: winners and losers. *Glob. Chang. Biol*. **21**, 1907–1913. (doi:10.1111/gcb.12841)
68. Glover CP, Kidwell SM. 1993 Influence of organic matrix on the post-mortem destruction of molluscan shells. *J. Geol*. **101**, 729–747. (doi:10.1086/648271)
69. Andersson A, Mackenzie F, Bates N. 2008 Life on the margin: implications of ocean acidification on Mg-calcite, high latitude and cold-water marine calcifiers. *Mar. Ecol. Prog. Ser*. **373**, 265–273. (doi:10.3354/meps07639)
70. Bischoff WD, Mackenzie FT, Bishop FC. 1987 Stabilities of synthetic magnesian calcites in aqueous solution: comparison with biogenic materials. *Geochim. Cosmochim. Acta* **51**, 1413–1423. (doi:10.1016/0016-7037(87)90325-5)
71. Long X, Ma Y, Qi L. 2014 Biogenic and synthetic high magnesium calcite—a review. *J. Struct. Biol*. **185**, 1–14. (doi:10.1016/j.jsb.2013.11.004)
72. Walter LM, Morse JW. 1985 The dissolution kinetics of shallow marine carbonates in seawater: a laboratory study. *Geochim. Cosmochim. Acta* **49**, 1503–1513. (doi:10.1016/0016-7037(85)90255-8)
73. Figuerola B, Griffiths HJ, Krzeminska M, Piwoni-Piorewicz A, Iglikowska A, Kuklinski P. 2023 Temperature as a likely driver shaping global patterns in mineralogical composition in bryozoans: implications for marine calcifiers under global change. *Ecography* **2023**, e06381. (doi:10.1101/2022.09.30.510275)
74. Milano S, Schöne BR, Witbaard R. 2017 Changes of shell microstructural characteristics of *Cerastoderma edule* (Bivalvia)—a novel proxy for water temperature. *Palaeogeogr. Palaeoclimatol. Palaeoecol*. **465**, 395–406. (doi:10.1016/j.palaeo.2015.09.051)
75. Lewis ER, Wallace DWR. 1998 Program developed for CO_2 system calculations. Oak Ridge, TN: Carbon Dioxide Information Analysis Center, US Department of Energy.
76. Zuur AF, Ieno EN, Elphick CS. 2010 A protocol for data exploration to avoid common statistical problems. *Methods Ecol. Evol*. **1**, 3–14. (doi:10.1111/j.2041-210x.2009.00001.x)
77. Bates D, Mächler M, Bolker B, Walker S. 2015 Fitting linear mixed-effects models using lme4. *J. Stat. Softw.* **67**, 1–48. (doi:10.18637/jss.v067.i01)
78. Bartoń K. 2025 Mumin: multi-model inference. See https://cran.r-project.org/web/packages/MuMIn/index.html.
79. Lenth RV. 2017 emmeans: estimated marginal means, aka least-squares means 2017:1.11.2-8. See https://doi.org/10.32614/CRAN.package.emmeans.
80. Kennish MJ, Lutz RA. 1999 Calcium carbonate dissolution rates in deep-sea bivalve shells on the East Pacific Rise at 21°N: results of an 8-year in-situ experiment. *Palaeogeogr. Palaeoclimatol. Palaeoecol*. **154**, 293–299. (doi:10.1016/s0031-0182(99)00102-9)

Downloaded from http://royalsocietypublishing.org/rsos/article-pdf/doi/10.1098/rsos.251473/5634029/rsos.251473.pdf
by guest
on 23 January 2026

81. Meier HEM, Kjellström E, Graham LP. 2006 Estimating uncertainties of projected Baltic Sea salinity in the late 21st century. *Geophys. Res. Lett*. **33**, L026488. (doi:10.1029/2006gl026488)
82. Vuorinen I *et al*. 2015 Scenario simulations of future salinity and ecological consequences in the Baltic Sea and adjacent North Sea areas—implications for environmental monitoring. *Ecol. Indic*. **50**, 196–205. (doi:10.1016/j.ecolind.2014.10.019)
83. Des M, Fernández-Nóvoa D, deCastro M, Gómez-Gesteira JL, Sousa MC, Gómez-Gesteira M. 2021 Modeling salinity drop in estuarine areas under extreme precipitation events within a context of climate change: effect on bivalve mortality in Galician Rías Baixas. *Sci. Total Environ*. **790**, 148147. (doi:10.1016/j.scitotenv.2021.148147)
84. Waller CL, Barnes DKA, Convey P. 2006 Ecological contrasts across an Antarctic land–sea interface. *Austral Ecol*. **31**, 656–666. (doi:10.1111/j.1442-9993.2006.01618.x)
85. Tunnicliffe V, Davies KTA, Butterfield DA, Embley RW, Rose JM, Chadwick WW. 2009 Survival of mussels in extremely acidic waters on a submarine volcano. *Nat. Geosci*. **2**, 344–348. (doi:10.1038/ngeo500)
86. Harper EM, Checa AG, Rodríguez-Navarro AB. 2009 Organization and mode of secretion of the granular prismatic microstructure of *Entodesma navicula* (Bivalvia: Mollusca). *Acta Zool*. **90**, 132–141. (doi:10.1111/j.1463-6395.2008.00338.x)
87. Addadi L, Joester D, Nudelman F, Weiner S. 2006 Mollusk shell formation: a source of new concepts for understanding biomineralization processes. *Chem. Eur. J*. **12**, 980–987. (doi:10.1002/chem.200500980)
88. Levi-Kalisman Y, Falini G, Addadi L, Weiner S. 2001 Structure of the nacreous organic matrix of a bivalve mollusk shell examined in the hydrated state using cryo-TEM. *J. Struct. Biol.* **135**, 8–17. (doi:10.1006/jsbi.2001.4372)
89. Marin F, Luquet G, Marie B, Medakovic D. 2007 Molluscan shell proteins: primary structure, origin, and evolution. *Curr. Top. Dev. Biol.* **80**, 209–276. (doi:10.1016/s0070-2153(07)80006-8)
90. Weiner S. 1979 Aspartic acid-rich proteins: major components of the soluble organic matrix of mollusk shells. *Calcif. Tissue Int*. **29**, 163–167. (doi:10.1007/bf02408072)
91. Hall A, Kennedy WJ, Taylor JH. 1997 Aragonite in fossils. *Proc. R. Soc. B* **168**, 377–412. (doi:10.1098/rspb.1967.0071)
92. Lagos NA *et al*. 2021 Plasticity in organic composition maintains biomechanical performance in shells of juvenile scallops exposed to altered temperature and pH conditions. *Sci. Rep*. **11**, 24201. (doi:10.1038/s41598-021-03532-0)
93. Checa AG, Rodríguez-Navarro AB. 2005 Self-organisation of nacre in the shells of Pterioida (Bivalvia: Mollusca). *Biomaterials* **26**, 1071–1079. (doi:10.1016/j.biomaterials.2004.04.007)
94. Kamat S, Su X, Ballarini R, Heuer AH. 2000 Structural basis for the fracture toughness of the shell of the conch *Strombus gigas*. *Nature* **405**, 1036–1040. (doi:10.1038/35016535)
95. Uozumi S, Iwata K, Togo Y. 1972 The ultrastructure of the mineral in and the construction of the crossed-lamellar layer in molluscan shell. *J. Fac. Sci. Hokkaido Univ. Ser. 4 Geol. Mineral.* **15**, 447–477.
96. Checa AG, Pina CM, Osuna-Mascaró AJ, Rodríguez-Navarro AB, Harper EM. 2014 Crystalline organization of the fibrous prismatic calcitic layer of the Mediterranean mussel *Mytilus galloprovincialis*. *Eur. J. Mineral*. **26**, 495–505. (doi:10.1127/0935-1221/2014/0026-2374)
97. Okumura T, Suzuki M, Nagasawa H, Kogure T. 2012 Microstructural variation of biogenic calcite with intracrystalline organic macromolecules. *Cryst. Growth Des*. **12**, 224–230. (doi:10.1021/cg200947c)
98. Palmer AR. 1992 Calcification in marine molluscs: how costly is it? *Proc. Natl Acad. Sci*. USA **89**, 1379–1382. (doi:10.1073/pnas.89.4.1379)
99. Morse JW, Andersson AJ, Mackenzie FT. 2006 Initial responses of carbonate-rich shelf sediments to rising atmospheric pCO_2 and 'ocean acidification': role of high Mg-calcites. *Geochim. Cosmochim. Acta* **70**, 5814–5830. (doi:10.1016/j.gca.2006.08.017)
100. King BF, Peck LS, Sokołowski A, Harper EM. Submitted. Low salinity limits size and affects shell thickness and shape in the lagoon cockle, *Cerastoderma glaucum* in the Baltic Sea.
101. Grenier C, Román R, Duarte C, Navarro JM, Rodriguez-Navarro AB, Ramajo L. 2020 The combined effects of salinity and pH on shell biomineralization of the edible mussel *Mytilus chilensis*. *Environ. Pollut*. **263**, 114555. (doi:10.1016/j.envpol.2020.114555)
102. Ramajo L, Prado L, Rodriguez-Navarro A, Lardies M, Duarte C, Lagos N. 2016 Plasticity and trade-offs in physiological traits of intertidal mussels subjected to freshwater-induced environmental variation. *Mar. Ecol. Prog. Ser*. **553**, 93–109. (doi:10.3354/meps11764)
103. King B. 2025 Bethany francesking/salinity_dissolution: salinity dissolution dataset (v1.0.0). Zenodo. (doi:10.5281/zenodo.17515481)
104. Li W. 2018 figshare. (doi:10.6084/m9.figshare.6025748)

Downloaded from http://royalsocietypublishing.org/rsos/article-pdf/doi/10.1098/rsos.251473/5634029/rsos.251473.pdf
by guest
on 23 January 2026